Characteristic Features in the Collision of Chemical Waves Depending on the Aspect Ratio of a Rectangular Field

Mariko Matsushita,[†] Satoshi Nakata,*[,†] and Hiroyuki Kitahata[‡]

Department of Chemistry, Nara University of Education, Takabatake-cho, Nara 630-8528, Japan, and Department of Physics, Graduate School of Science, Kyoto University, Kyoto 606-8502, Japan

Received: November 30, 2006; In Final Form: April 20, 2007

The photosensitive Belousov−Zhabotinsky (BZ) reaction was investigated on a double rectangular field composed of two rectangular routes, which was drawn using computer software and then projected using a liquid-crystal projector on a filter paper soaked with BZ solution. When two chemical waves were generated on the rectangular routes as the initial condition, the nature of the collision of the waves could be theoretically classified into four categories depending on the initial phase difference between the two waves and the aspect ratio of the rectangular routes. The experimental results were consistent with the features of the theoretical prediction. These results suggest that the feature of wave propagation characteristically develops depending on the geometry of the excitable fields.

Introduction

Experimental and theoretical studies on wave propagation on excitable media may help us not only to understand signal processing in biological systems[1] such as nerve impulses,[2,3] but also to create novel methods for artificial processing such as image processing[4−7] and information processing[8−13] based on a reaction-diffusion system. Various features of wave propagation and oscillation have been experimentally and theoretically investigated with the Belousov−Zhabotinsky (BZ) reaction as an excitable or oscillatory chemical system.[14−16] In addition, there have been many studies on the features of wave propagation on excitable fields with various geometries.[17−24]

A photosensitive experimental setup for the BZ reaction[4,5,12,25,26] makes it easier to create excitable fields with various geometries, which are drawn by computer software and then projected on a filter paper soaked with BZ solution using a liquid-crystal projector which was drawn by computer software. Using a liquid-crystal projector, the shape is projected on a filter paper soaked with BZ reaction.[13,27] In this case, light illumination produces bromine which inhibits the oscillatory reaction; i.e., the degree of excitability can be adjusted by changing the intensity of illumination. Therefore, the number of chemical waves and their locations can be spatio-temporally regulated by the local illumination of unwanted waves.[13,28]

We have recently reported interactive propagation of chemical waves on a figure-eight field composed of two equivalent circular rings illuminated with a liquid-crystal projector.[29,30] When two chemical waves were generated on the figure-eight field, the locations at which the waves collided were constant for slightly connected rings and alternated for rings that completely overlapped. In addition, we have reported experimentally and theoretically that there are two categories of collision depending on the initial phase difference between two waves ($\Delta\theta_{\mathrm{ini}}$) for slightly connected rings (i.e., in one case the final phase difference is determined by $\Delta\theta_{\mathrm{ini}}$, and in the other case it is constant and independent of $\Delta\theta_{\mathrm{ini}}$) and that the critical value of $\Delta\theta_{\mathrm{ini}}$ depends on the thickness of the ring. However, the amplitude of the alternating collision and the effect of the degree of overlap have not yet been clarified.

Therefore, in the present study, we examined the characteristic features of collision on the wave propagation as a continuation of our previous study. We used a double rectangular field as a figure-eight field in place of equivalent circular rings to clarify the influence of the degree of overlap. When two chemical waves were initially generated on the double rectangular routes (i.e., one wave for each rectangular route), four categories of wave collision could be distinguished depending on the initial phase difference between the two waves and the aspect ratio of a single rectangular route. The presence of the four categories was derived in a theoretical way. We can regard that the information on the chemical wave is remained, if we can know the initial condition from the present condition. Thus, this might be an interesting problem from the viewpoint of informatics.

Experimental Theory

We discuss interactive chemical wave propagation on a double rectangular field which was made by partly overlapping two equivalent rectangular routes, $\mathbf{F}_1$ as an upper route and $\mathbf{F}_2$ as a lower one, as shown in Figure 1a-1. The horizontal length of the inner boundary and the width of the rectangular route were defined as na and a, respectively. Thus, a was the fundamental length, and n was the aspect ratio of the region **PQRS**, which was equal to that of the inner boundary of the single rectangular route. Figure 1a-2 shows the definition of the phase and corner-points (**P**, **Q**, **R**, and **S**) along the inner boundaries of the individual rectangular routes. Here, l_i ($i = 1$, 2) is the coordinate along the inner rectangular boundary from the origin, $\mathbf{O}_i$, for $\mathbf{F}_i$. The phase θ_i for the chemical wave $\mathbf{W}_i$ on a closed route is defined as

$$\theta_i = \frac{l_i}{a(n+1)} \tag{1}$$

* To whom correspondence should be addressed. Tel. and fax: +81-742-27-9191. E-mail: nakatas@nara-edu.ac.jp.
† Nara University of Education.
‡ Kyoto University.

10.1021/jp068207n CCC: $37.00
Published on Web 06/08/2007

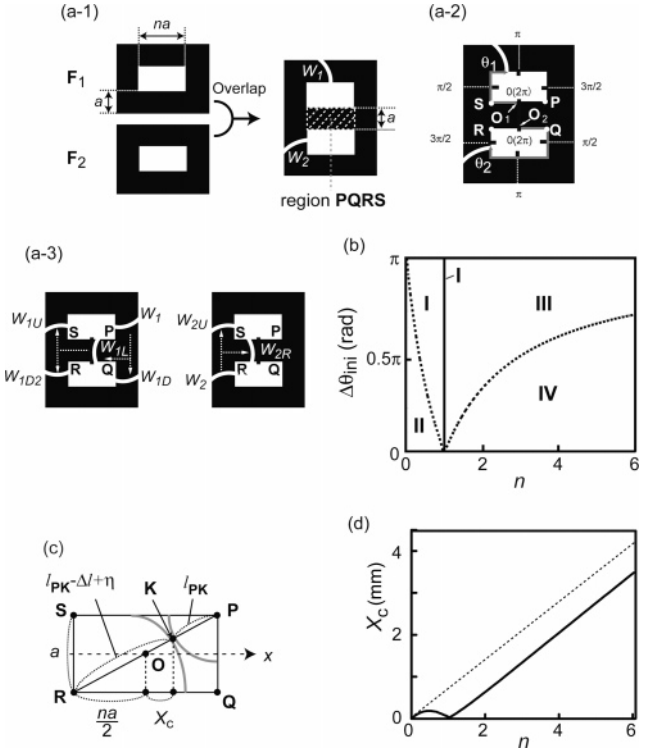

Figure 1. Theoretical prediction of the features of wave propagation on a double rectangular field based on eqs 1−6. (a-1) Double rectangular field composed of $\mathbf{F}_1$ and $\mathbf{F}_2$, and definitions for $\mathbf{O}_i$, $\mathbf{W}_i$, *na*, and *a*. (a-2) Definitions for points **P**, **Q**, **R**, and **S** at the region **PQRS** and the phase, θ_i. (b) Phase diagram of the categories of collision (**I**, **II**, **III**, and **IV**) in $n-\Delta\theta_{ini}$ space. Dotted curves, which were derived based on eq 2, are the boundaries between **III** and **IV** for $n > 1$ and between **I** and **II** for $0 < n \leq 1$. (c) Schematic diagram to derive the locations of collision, X_c, at the region **PQRS**. (d) Location of collision, X_c, depending on *n* for categories **I** ($0 < n \leq 1$) and **III** ($1 < n$) based on eq 5 ($\eta = 0$). The dotted line in panel d corresponds to the location of **P**. The dotted line in panel d corresponds to the location of **P**. The parameter *a* is set as 1.9 mm.

where $2a(n + 1)$ is the peripheral length of the inner boundary of the single rectangular route which corresponds to 2π. Hereafter, the phases are represented in radians.

Next, we consider the case in which two chemical waves, $\mathbf{W}_1$ and $\mathbf{W}_2$, propagate clockwise and collide on the double rectangular field. A photosensitive chemical wave on a circular ring propagates with an almost equivalent velocity[20] and its shape is well approximated as the involute of the circle.[20,31−34] Due to the symmetry of $\mathbf{F}_1$ and $\mathbf{F}_2$, we only need to consider when $\Delta\theta_{ini} \geq 0$ ($\Delta\theta_{ini}$: initial phase difference, where $\Delta\theta = \theta_1 - \theta_2$). If we do not consider collision between $\mathbf{W}_1$ and $\mathbf{W}_2$, $\mathbf{W}_1$ can diverge to the left ($\mathbf{W}_{1L}$) and downward ($\mathbf{W}_{1D}$) from **Q**, $\mathbf{W}_{1L}$ can diverged upward ($\mathbf{W}_{1U}$) and downward ($\mathbf{W}_{1D2}$) from **R**, and $\mathbf{W}_2$ can diverge to the right ($\mathbf{W}_{2R}$) and upward ($\mathbf{W}_{2U}$) from **S**. If $\Delta\theta_{ini} = 0$, $\mathbf{W}_1$ and $\mathbf{W}_2$ collide at the center of the field for every collision.

When $\mathbf{W}_{1L}$ reaches **S** before $\mathbf{W}_2$, $\mathbf{W}_{1U}$ in the upper direction is remained due to divergence from **R**, but $\mathbf{W}_2$ disappears upon collision with $\mathbf{W}_{1D2}$ which diverges downward. In this case, the initial information for $\mathbf{W}_2$, i.e., θ_{ini} of $\mathbf{W}_2$, is lost after the collision. In contrast, when $\mathbf{W}_2$ reaches **S** earlier than $\mathbf{W}_{1L}$, $\mathbf{W}_2$ is remained, but $\mathbf{W}_{2R}$ and $\mathbf{W}_{1L}$ disappear upon collision between them. Thus, if $\mathbf{W}_2$ reaches **S** before $\mathbf{W}_{1L}$ does, the initial information for $\mathbf{W}_2$ is remained after the collision, otherwise, this information is lost. Thus, the competition between $\mathbf{W}_1$ and $\mathbf{W}_2$ to reach a certain point determines whether or not the initial phase difference is remained.

TABLE 1: Categorization on the Features of Collision from the Viewpoint of the Initial Information of Chemical Wave Propagation

information	lost	remained
$n \leq 1$	**I**	**II**
$n > 1$	**III**	**IV**

Here, we will show that there are four categories of collision (**I**, **II**, **III**, and **IV**) depending on $\Delta\theta_{ini}$. To clarify the discussion, we consider the case in which $\mathbf{W}_1$ is initially located at **P** ($l_1 = (1.5n + 2)a$).

For $0 < n < 1$, $\mathbf{W}_1$ reaches **Q** after it passes through **S**. Here, we consider the case in which $\mathbf{W}_1$ and $\mathbf{W}_2$ reach **Q** at the same time. In this case, $\mathbf{W}_2$ is located at $l_2 = (2.5n + 1)a$ when $\mathbf{W}_1$ is located at **P**, i.e., $\Delta l_{ini} = (1 - n)a$. If $\Delta l_{ini} > (1 - n)a$, the initial information for $\mathbf{W}_1$ remains, but that for $\mathbf{W}_2$ is lost since $\mathbf{W}_1$ reaches **Q** before $\mathbf{W}_2$ does. The location of the collision is constant after the second collision. Here, this collision is distinguished as category **I**. In contrast, if $\Delta l_{ini} < (1 - n)a$, the initial information for $\mathbf{W}_2$ is remained since $\mathbf{W}_2$ reaches **Q** before $\mathbf{W}_1$ does. The location of the collision is fixed after the first collision. Here, this collision is distinguished as category **II**. Thus, $\Delta l_{ini} = (1 - n)a$ is the critical value between categories **I** and **II**. In other words, $\Delta\theta_c = \pi(1- n)/(n + 1)$ is the critical value for the phase description in eq 1.

For $n > 1$, we consider the case in which $\mathbf{W}_{1L}$ and $\mathbf{W}_2$ reach **S** at the same time. In this case, $\mathbf{W}_2$ is located at $l_2 = (0.5n + 3)a$ when $\mathbf{W}_1$ is located at **P**, i.e., $\Delta l_{ini} = (n - 1)a$, where l_{ini} is the initial value of l_i ($i = 1$ or 2), and $\Delta l = l_1 - l_2$. If $\Delta l_{ini} > (n - 1)a$, the initial information for $\mathbf{W}_1$ is remained but that for $\mathbf{W}_2$ is lost since $\mathbf{W}_{1L}$ reaches **S** before $\mathbf{W}_2$ does. After the first collision, collision occurs between $\mathbf{W}_{1L}$ and $\mathbf{W}_{1D}$ (newly defined as $\mathbf{W}_2$), and the location of this collision alternates between two points that are symmetrical with regard to **O** (see Figure 1c). Here, this collision is classified as category III. In contrast, if $\Delta l_{ini} < (n - 1)a$, the initial information for $\mathbf{W}_2$ is remained and collision between $\mathbf{W}_1$ and $\mathbf{W}_2$ is repeated at the region **PQRS** since $\mathbf{W}_2$ reaches **S** before $\mathbf{W}_{1L}$ does. The location of collision alternates between two points that are symmetrical with regard to the center of the field inside the region **PQRS**. Here, this collision is classified as category **IV**. $\Delta l_{ini} = (n - 1)a$ is the critical value between categories **III** and **IV**. Thus, $\Delta\theta_c = \pi(n - 1)/(n + 1)$ is the critical phase difference.

For $n = 1$, $\mathbf{W}_2$ disappears after the first collision with $\mathbf{W}_{1L}$, and therefore the initial information (θ_{ini}) for $\mathbf{W}_2$ is lost. The second collision occurs between $\mathbf{W}_{1L}$ and new $\mathbf{W}_2$ (or $\mathbf{W}_{1D}$) for every $\Delta\theta_{ini}$ (>0), i.e., $\Delta\theta = 0$ for the second collision. Thus, the collision at the center of the field around $\theta = 0$ is maintained after the second collision. Here, this collision is distinguished as category I since the feature of collision is similar to that for $0 < n < 1$.

By combining these results, we write

$$\begin{cases} \Delta\theta_{ini} < \Delta\theta_c & \text{(information for } \mathbf{W}_2 \text{ is remained; categories } \mathbf{II} \text{ and } \mathbf{IV}) \\ \quad \geq \Delta\theta_c & \text{(information for } \mathbf{W}_2 \text{ is lost; categories } \mathbf{I} \text{ and } \mathbf{III}) \\ \Delta\theta_c = \dfrac{|1 - n|}{n + 1}\pi & \end{cases} \tag{2}$$

and the phase diagram for the collision category based on eq 2 is shown in Figure 1b and Table 1.

Next, we consider the location of collision. For cases in which the initial information for $\mathbf{W}_2$ is lost, i.e., categories **I** and **III**,

the second collision occurs between $\mathbf{W}_1$ and new $\mathbf{W}_2$ at the region **PQRS** since the initial $\mathbf{W}_2$ disappears upon the first collision with $\mathbf{W}_{1L}$ for $n \geq 1$ or $\mathbf{W}_1$ for $0 < n < 1$. When $\mathbf{W}_{1L}$ arrives at $\mathbf{O}_1$ ($l_1 = 0$), $\mathbf{W}_{1D}$, which is diverged from $\mathbf{W}_1$ at **Q**, is located at $l_2 = (n-1)a$. Thus, the phase difference between $\mathbf{W}_{1L}$ and new $\mathbf{W}_2$ (or $\mathbf{W}_{1D}$) is

$$\Delta\theta = \theta_1 - \theta_2 = -\frac{l_1 - l_2}{a(n+1)}\pi = -\frac{n-1}{n+1}\pi \qquad (3)$$

For cases in which the initial information for $\mathbf{W}_2$ is remained, i.e., categories **II** and **IV**, the location of the collision is determined by the initial phase difference between $\mathbf{W}_1$ and $\mathbf{W}_2$. On the other hand, for categories **I** and **III**, the two chemical waves, $\mathbf{W}_1$ and new $\mathbf{W}_2$, collide on the line **PR** upon and after the second collision. We set **K** as the collision point, **O** as the intersection between the line **PR** and the *x*-axis, and $l_{\mathbf{PK}}$ as the distance between **P** and **K**, as shown in Figure 1c.

The projected length of $l_{\mathbf{OK}}$ on the *x*-axis, X_c, can be expressed as

$$X_c = \frac{n}{2\sqrt{n^2+1}}\left(\frac{a(n+1)|\Delta\theta|}{\pi} + \eta\right) \qquad (4)$$

where X_c corresponds to the amplitude of the alternate collision on the *x*-axis for category **III** or the converged location of collision on the *x*-axis for category **I,** and η is the effect of the corner on the chemical wave propagation (see Appendix). Inserting $\Delta\theta$ (see eq 3), we obtain

$$X_c = \frac{n}{2\sqrt{n^2+1}}|a(n-1) + \eta| \qquad (5)$$

This dependence of X_c on *n* in the case of $\eta = 0$ is shown in Figure 1d. Equation 5 indicates that X_c for categories **I** and **III** is determined by *n*.

We can consider these phenomena using the following mapping between $\Delta\theta_k$ and $\Delta\theta_{k+1}$ ($\Delta\theta_k$ is the phase difference when the chemical waves collide *k* times) for $\eta = 0$ is expressed as

$$\begin{cases} \Delta\theta_{k+1} = -\Delta\theta_k \,\mathrm{sign}(n-1) & \text{if } |\Delta\theta_k| < \Delta\theta_c \quad \text{(information for } \mathbf{W}_2 \text{ is remained)} \\ = -\dfrac{n-1}{n+1}\pi \,\mathrm{sign}(\Delta\theta_k) & \text{if } |\Delta\theta_k| \geq \Delta\theta_c \quad \text{(information for } \mathbf{W}_2 \text{ is lost)} \end{cases} \qquad (6)$$

where sign(*y*) is equal to 1 for $y > 0$, to 0 for $y = 0$, and to -1 for $y < 0$.

Equation 6 indicates that the location of the collision alternates for every collision with a constant amplitude (original point: $l = 0$) for $n > 1$, and that it converges for $n \leq 1$.

Experiments

$Ru(bpy)_3Cl_2$, which was purchased from Sigma-Aldrich (St. Louis, MO), was used as a catalyst for the photosensitive BZ reaction. The BZ solution consisted of $[NaBrO_3] = 0.51$ M, $[H_2SO_4] = 0.34$ M, $[CH_2(COOH)_2] = 0.16$ M, $[KBr] = 0.01$ M, and $[Ru(bpy)_3Cl_2] = 1.7$ mM. A cellulose nitrate membrane filter (Advantec, A100A025A, diameter of the membrane = 25 mm) with a pore size of 1 μm was homogeneously soaked in BZ solution (5 mL) for about 1 min. The soaked membrane filter was gently wiped with another pure filter paper to remove excess solution and placed on a glass plate ($77 \times 52 \times 1.3$ mm^3). The surface of the membrane filter was completely covered with 1 mL silicone oil (Wako, WF-30) to prevent it from drying and to protect it from the influence of oxygen in air. The experiments were carried out in an air-conditioned room at 298 ± 2 K, at which the reaction medium showed no oscillation and exhibited almost constant wave propagation behavior for approximately 30 min.

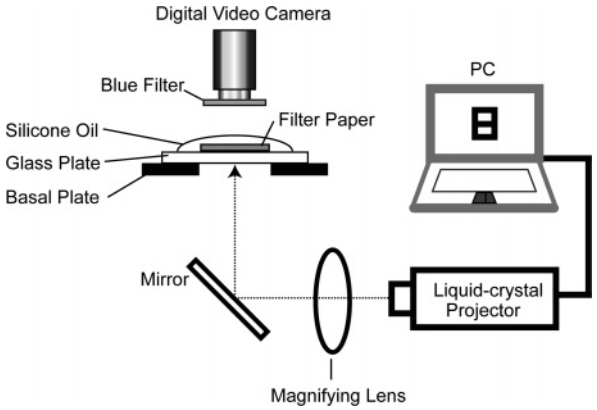

Figure 2. Schematic illustration of the experimental system based on the photosensitive BZ reaction.

The medium was illuminated from below as schematically shown in Figure 2. The high-pressure mercury bulb of a liquid-crystal projector (Mitsubishi, LPV-XL8) was used as a light source, the spatial intensity distribution was controlled with a personal computer, and a magnifying lens was used to adjust the focus. The black and white picture created by the liquid-crystal projector served as an illumination mask to create the appropriate boundary. The light intensities on the black and white regions were 4.0×10^2 and 1.7×10^4 lx, respectively, where the light intensity at the illuminated part was measured with a light intensity meter (Asone, LX-100). Actually, *a* in Figure 1a-1 was 1.9 mm, and *n* was changed between 0.5 and 6.0. The velocity of the chemical wave at the inner boundary of the single rectangular route was maintained at ca.0.07 mm/s except at the corner.

To prepare a unidirectional chemical wave on each rectangular route and adjust the initial phase difference between the two waves, the following processes were performed. (1) Several chemical waves were initially generated on the excitable field under no illumination, i.e., dark condition. (2) When illumination except in the dark area was started, the chemical waves disappeared in the illuminated area but maintained in the unilluminated reaction field. (3) Unwanted waves disappeared upon local illumination. (4) To adjust the initial phase difference between two waves, another chemical wave was translated from another darker area to the rectangular routes. Thus, we prepared the experimental conditions so that two chemical waves propagate in a clockwise direction to simplify the discussions on the nature of the collision of two waves.

The experiments were monitored from above with a digital video camera (Sony DCR-VX700) and recorded on videotape. A blue optical filter (Asahi Techno Glass, V-42) with a maximum transparency at 410 nm was used to enhance the images of the green-colored chemical waves, which correspond to the oxidized state, $[Ru(bpy)_3]^{3+}$.

Results and Discussion

Figure 3 shows snapshots of wave propagation on the double rectangular fields with different *n* for various initial phase differences. For $n = 1$, $\mathbf{W}_{1L}$ and $\mathbf{W}_{1D}$ collided at around **O** on

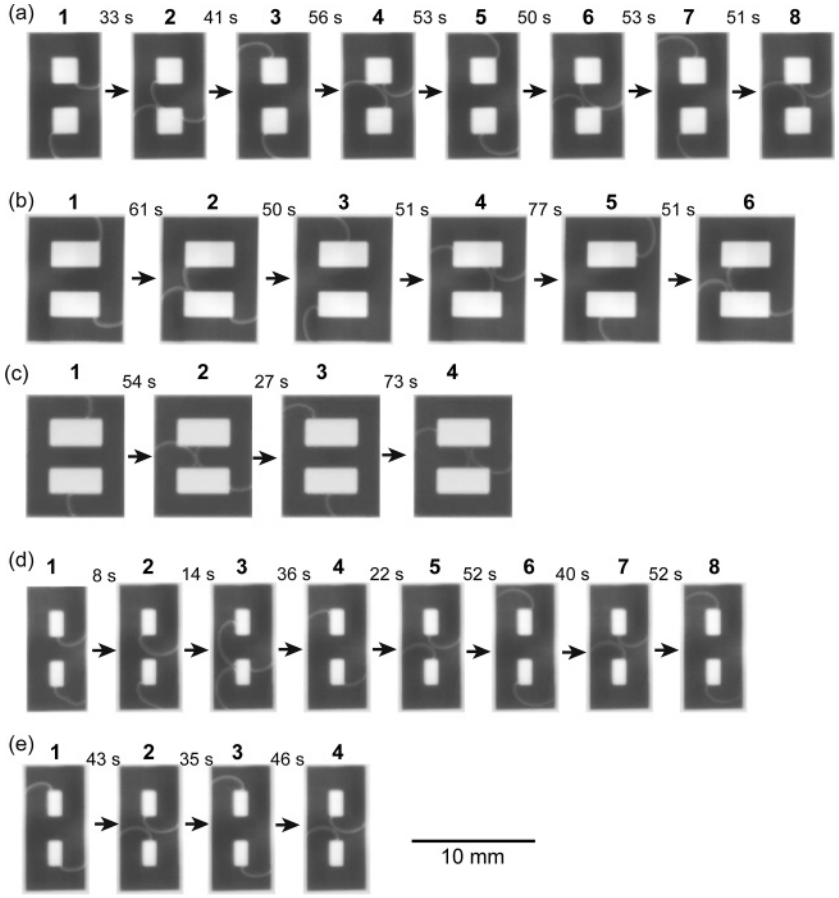

Figure 3. Experimental results for snapshots of wave propagation on a double rectangular field for different n ((a) $n = 1$, (b, c) $n = 2$, (d, e) $n = 0.5$). After the first collision, the initial information for $\mathbf{W}_2$ disappeared in panels a, b, and d but remained in panels c and e. Time intervals between the individual snapshots are shown. $\Delta\theta_{ini}$ values were (a) 0.5π, (b) 0.6π, (c) 0.1π, (d) $0.8\ \pi$, and (e) $0.1\ \pi$.

and after the second collision, as seen in Figure 3a. With the increase in the number of collisions, the location of collision was almost at the center **O**, i.e., category **I** was observed.

For $n > 1$, two categories of collision were observed (Figures 3b and 3c). In one type, the initial information for $\mathbf{W}_2$ was lost; i.e., $\mathbf{W}_2$ disappeared upon collision with $\mathbf{W}_{1L}$, as seen in snapshot 2 in Figure 3b. The second collision occurred between $\mathbf{W}_{1L}$ and $\mathbf{W}_{1D}$ (snapshots 3 and 4). In this category, the location of collision alternated between the left and right edges of the region **PQRS** (snapshots 2, 4, 6), i.e., category **III** was observed. In the other type of collision, the initial information for $\mathbf{W}_1$ and $\mathbf{W}_2$ was remained after the collision, as shown in Figure 3c. In this category, the location of the collision was alternated around the inner side of the region **PQRS** (snapshots 2, 4). Thus, category **IV** was observed.

For $0 < n < 1$, two categories of collision, for which the location of collision was constant, were observed. In the category shown in Figure 3d, $\mathbf{W}_2$ disappeared upon the first collision at around **R** (snapshot 2), and then collision between $\mathbf{W}_{1L}$ and $\mathbf{W}_{1D}$ was observed on and after the second collision (snapshots 3−7). Thus, category **I** was observed. In the other category shown in Figure 3e, $\mathbf{W}_1$ collided with $\mathbf{W}_2$ at around $\theta = 0$ upon the first collision (snapshot 2), and $\mathbf{W}_{1U}$ in the upward direction and $\mathbf{W}_{2R}$ in the right direction were remained (snapshots 3, 4). The location of collision was maintained on and after the first collision. Thus, category **II** was observed.

Here, we consider the effect of corners on the chemical wave. The effect of corners is counteracted for categories **II** and **IV** since $\mathbf{F}_1$ is equivalent to $\mathbf{F}_2$. That is, we can see no effect of corners. In contrast, the symmetry is broken when the two

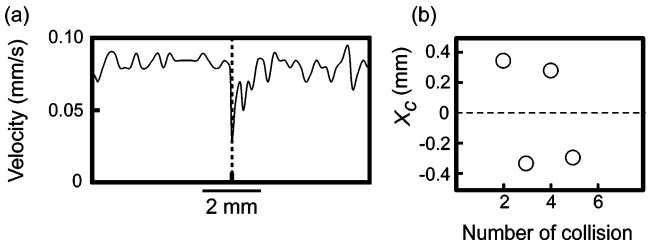

Figure 4. Experimental results for (a) migration length vs velocity of a chemical wave when it turned a corner, and (b) X_c, depending on the number of collision between $\mathbf{W}_{1L}$ and $\mathbf{W}_{1D}$ after the first collision. The chemical wave passed through the corner at the time indicated by the dotted line in panel a.

chemical waves turn the different number of corners for categories **I** and **III**. We discuss the effect of corners by considering the delay length, Δl_c, which is generated when the chemical wave turns the corner. The velocity of the chemical wave, v, was decreased when it turned the corner, as shown in Figure 4a. Δl_c for one corner was estimated as 0.38 mm by $\int_{t_1}^{t_2} (v_{av} - v(t))\ dt$, where v_{av} was the average velocity when the chemical wave propagated straightforward, where t_1 and t_2 were the times before and after the chemical wave turned the corner, respectively. As shown in Figures 3 and 4b, X_c was not completely zero but alternately changed with the amplitude of 0.32 ± 0.05 mm. Thus, the amplitude of collision location including the effect of corners ($|X_c|$) is calculated as $\Delta l_c/\sqrt{2} = 0.26$ for $n = 1$ (see Appendix). Thus, $|X_c|$ for $n = 1$ obtained from Figure 4b is similar to that in eq 10. As for $n > 1$, the effect of corner decreases with the increase in n, as suggested in eq 5. As for the effect of corners for category **I** for $n < 1$, X_c

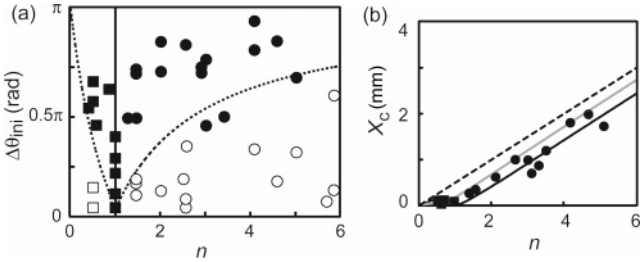

Figure 5. Experimental results for (a) the phase diagram of the four categories of collision (**I**, filled square; **II**, empty square; **III**, filled circle; **IV**, empty circle) and (b) the location of collision, X_c, depending on n for categories **I** ($0 < n \leq 1$) and **III** ($1 < n$) with (solid gray line, $\Delta l_c = 0.3$ mm) and without (solid black line, $\Delta l_c = 0$) the effect of the corner. The parameter except in the dark area a is set at 1.9 mm. The curves in panels a and b correspond to those in panels b and d in Figure 1, respectively.

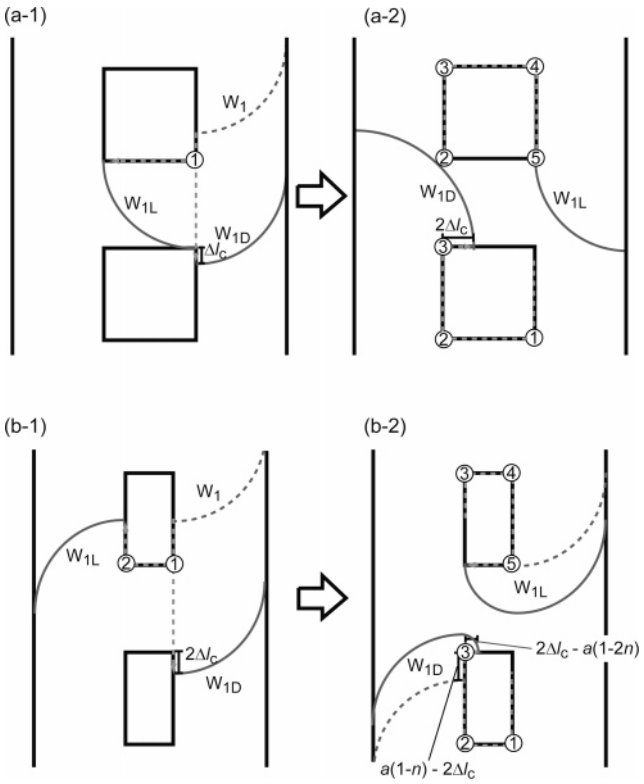

Figure 6. Schematic illustration on the wave propagation on a double rectangular from (1) divergence of $\mathbf{W}_1$ to (2) collision between $\mathbf{W}_{1L}$ and $\mathbf{W}_{1D}$ for (a) $n \geq 1$ and (b) $n < 1$. The numbers in the empty circles indicate the count on turning the corner for $\mathbf{W}_{1L}$ and $\mathbf{W}_{1D}$.

is reduced since $a(n - 1) < 0$ but $\Delta l_c > 0$, as suggested in eq 5 (see Appendix).

Figure 5 shows a comparison of the experimental and theoretical results for (a) the classification of the four categories of collision (**I**, **II**, **III**, and **IV**) and (b) the relationship between X_c and n for categories **I** ($0 < n \leq 1$) and **III** ($1 < n$). In Figure 4a, the experimental data nearly coincide with the classification based on eq 2. The three contradictory data around the boundary between categories **III** and **IV**, and the convergence to $\theta = 0$ for $n = 1$ with time (see Figure 3a), may be the result of the experimental precision, e.g., the effect of corners on the velocity of the wave propagation because of the slight leak of the inhibitor from the bright to the dark region. In Figure 4b, experimental data for X_c are approximated by the theoretical curves based on eq 5. Thus, the experimental results are well reproduced by the theoretical prediction.

Conclusion

The nature of wave propagation and collision in the photosensitive BZ reaction on an excitable double rectangular field illuminated with a liquid-crystal projector was examined. The collisions of chemical waves can be classified into four categories depending on the initial phase difference between the two waves ($\Delta\theta_{ini}$) and the aspect ratio of the single rectangular route (n). The results approximately correspond to the theoretical prediction.

The photosensitive BZ reaction may be useful for studying spatiotemporal development that depends on the geometric condition of the excitable fields since the shape of the reaction field can be varied using a personal computer. In addition, the features of wave propagation can be theoretically predicted because of the equal velocities of wave propagation during ca. 30 min of the experiments. To investigate the reaction fields with further complex shapes or to reproduce the theoretical prediction in the experiments, the development of an experimental system in place of immersed filter paper will be necessary to maintain and stabilize the velocity and features of wave propagation.

Appendix

Here, we derive eq 4 and consider the collision location and the effect of corner on the chemical wave. As $l_{\mathbf{PR}} \times (na/2 + X_c) = l_{\mathbf{QR}} \times l_{\mathbf{KR}}$, eq 7 is given (see Figure 1c):

$$a\sqrt{n^2+1}\left(\frac{na}{2} + X_c\right) = na(l_{\mathbf{PK}} - \Delta l + \eta) \tag{7}$$

Equation 8 is derived from eq 7:

$$X_c = -\frac{na}{2} + \frac{n}{\sqrt{n^2+1}}(l_{\mathbf{PK}} - \Delta l + \eta) \tag{8}$$

Since the distance between **P** and **R**, $a\sqrt{n^2+1}$, is equal to $2l_{\mathbf{PK}} - \Delta l + \eta$, we obtain

$$l_{\mathbf{PK}} = \frac{a}{2}\left(\sqrt{n^2+1} + \frac{(n+1)}{\pi}\Delta\theta - \frac{\eta}{a}\right) \tag{9}$$

Thus, eq 4 is obtained from eqs 8 and 9.

Next, we consider the effect of corners on the chemical wave propagation for categories **I** and **III**. We suppose that the delay length Δl_c is generated between $\mathbf{W}_{1L}$ and $\mathbf{W}_{1D}$, as shown in Figure 6. The numbers of corner which $\mathbf{W}_{1L}$ and $\mathbf{W}_{1D}$ turn are 5 and 3 from the divergence of $\mathbf{W}_1$ to the second collision between them at the region **PQRS**, i.e., η is equal to $2\Delta l_c$ on the second collision for **III** (see Figure 6a). As for **I**, the delay length is $2\Delta l_c - a(1 - n)$ on the second collision, as shown in Figure 6b. Therefore, eq 5 is rewritten as eq 10 if we consider the effect of the corners:

$$X_c = \frac{n}{2\sqrt{n^2+1}}|a(n-1) + 2\Delta l_c| \tag{10}$$

Acknowledgment. The authors thank Professor Yoshihito Mori (Ochanomizu Univerisity, Japan) and Professor Takatoshi Ichino (Kinki University, Japan) for their kind suggestions and comments. This work was supported in part by Grants-in-Aid for Scientific Research (No. 18550126) to S.N. and for Young

Scientists (No. 18740231) to H.K. from the Ministry of Education, Culture, Sports, Science, and Technology of Japan.

References and Notes

(1) Winfree, A. T. *The Geometry of Biological Time*; Springer: Berlin, 1980.
(2) Hall, Z. W., Ed. In *An Introduction to Molecular Neurobiology*; Sinauer: Sunderland, MA, 1992.
(3) Murray, J. D. *Mathematical Biology*; Springer: Berlin, 1989.
(4) Kuhnert, L. *Nature* **1986**, *319*, 393.
(5) Kuhnert, L.; Agladze, K. I.; Krinsky, V. I. *Nature* **1989**, *337*, 244.
(6) Rambidi, N. G.; Shamayaev, K. E.; Peshkov, G. Y. *Phys. Lett. A* **2002**, *298*, 375.
(7) Sakurai, T.; Mihaliuk, E.; Chirila, F.; Showalter, K. *Science* **2002**, *296*, 2009.
(8) Tóth, Á.; Showalter, K. *J. Chem. Phys.* **1995**, *103*, 2058.
(9) Steinbock, O.; Kettunen, P.; Showalter, K. *J. Phys. Chem.* **1996**, *100*, 18970.
(10) Motoike, I.; Yoshikawa, K. *Phys. Rev. E* **1999**, *59*, 5354.
(11) Ichino, T.; Igarashi, Y.; Motoike, N. I.; Yoshikawa, K. *J. Chem. Phys.* **2003**, *118*, 8185.
(12) Gorecka, J.; Gorecki, J. *Phys. Rev. E* **2003**, *67*, 067203.
(13) Nagahara, H.; Ichino, T.; Yoshikawa, K. *Phys. Rev. E* **2004**, *70*, 036221.
(14) Zaikin, A. N.; Zhabotinsky, A. M. *Nature* **1970**, *225*, 535.
(15) Field, R. J., Burger, M., Eds. In *Oscillations and Traveling Waves in Chemical Systems*; Wiley, New York, 1985.
(16) Kapral, R., Showalter, K., Eds. In *Chemical Waves and Patterns*; Kluwer Academic: Dordrecht, The Netherlands, 1995.
(17) Lázár, A.; Noszticzius, Z.; Försterling, H.-D.; Nagy-Ungvárai, Z. *Phys. D* **1995**, *84*, 112.
(18) Steinbock, O.; Kettunen, P.; Showalter, K. *Science* **1995**, *269*, 1857.
(19) Winston, D.; Arora, M.; Maselko, J.; Gáspár, V.; Showalter, K. *Nature* **1991**, *351*, 132.
(20) Iguchi, Y.; Takitani, R.; Miura, Y.; Nakata, S. *Rec. Res. Dev. Pure Appl. Chem.* **1998**, *2*, 113.
(21) Motoike, I. N.; Yoshikawa, K,; Iguchi, Y.; Nakata, S. *Phys. Rev. E* **2001**, *63*, 036220.
(22) Agladze, K.; Aliev, R. R.; Yamaguchi, T.; Yoshikawa, K. *J. Phys. Chem.* **1996**, *100*, 13895.
(23) Aliev, R. R.; Agladze, K. I. *Phys. D* **1991**, *50*, 65.
(24) Yoshida, R.; Takahashi, T.; Yamaguchi, T.; Ichijo, H. *J. Am. Chem. Soc.* **1996**, *118*, 5134.
(25) Kádár, S.; Amemiya, T.; Showalter, K. *J. Phys. Chem. A* **1997**, *101*, 8200.
(26) Agladze, K.; Tóth, Á.; Ichino, T.; Yoshikawa, K. *J. Phys. Chem. A* **2000**, *104*, 6677.
(27) Gorecki, J.; Yoshikawa, K.; Igarashi, Y. *J. Phys. Chem. A* **2003**, *107*, 1664.
(28) Amemiya, T.; Kádár, S.; Kettunen, P.; Showalter, K. *Phys. Rev. Lett.* **1996**, *77*, 3244.
(29) Kitahata, H.; Yamada, A.; Nakata, S.; Ichino, T. *J. Phys. Chem. A* **2005**, *109*, 4973.
(30) Nakata, S.; Morishima, S.; Kitahata, H. *J. Phys. Chem. A* **2006**, *110*, 3633.
(31) Müller, S. C.; Plesser, T.; Hess, B. *Phys. D* **1987**, *24*, 87.
(32) Volford, A.; Simon, P. L.; Farkas, H.; Noszticzius, Z. *Phys. A* **1999**, *274*, 30.
(33) Lázár, A.; Noszticzius, Z.; Farkas, H.; Försterling, H.-D. *Chaos* **1995**, *5*, 443.
(34) Lázár, A.; Försterling, H.-D.; Farkas, H.; Simon, P.; Volford, A.; Noszticzius, Z. *Chaos* **1997**, *7*, 731.